

# Revisiting constraints on the maximum neutron star mass in light of GW190814

Yeunhwan Lim,<sup>1,2,3,\*</sup> Anirban Bhattacharya,<sup>4,†</sup> Jeremy W. Holt,<sup>5,6,‡</sup> and Debdeep Pati<sup>4,§</sup>

<sup>1</sup>Max-Planck-Institut für Kernphysik, Saupfercheckweg 1, 69117 Heidelberg, Germany

<sup>2</sup>Institut für Kernphysik, Technische Universität Darmstadt, 64289 Darmstadt, Germany

<sup>3</sup>ExtreMe Matter Institute EMMI, GSI Helmholtzzentrum für Schwerionenforschung GmbH, 64291 Darmstadt, Germany

<sup>4</sup>Department of Statistics, Texas A&M University, College Station, TX 77843, USA

<sup>5</sup>Cyclotron Institute, Texas A&M University, College Station, TX 77843, USA

<sup>6</sup>Department of Physics and Astronomy, Texas A&M University, College Station, TX 77843, USA

(Dated: July 16, 2020)

We investigate the maximum neutron star mass based on constraints from low-energy nuclear physics, neutron star tidal deformabilities from GW170817, and simultaneous mass-radius measurements of PSR J0030+045 from NICER. Our prior distribution is based on a combination of nuclear modeling valid in the vicinity of normal nuclear densities together with the assumption of a maximally stiff equation of state at high densities. The transition density is treated as a model parameter with uniform prior. Bayesian likelihood functions involving measured neutron star tidal deformabilities and radii are subsequently used to generate equation of state posteriors. We demonstrate that a modification of the highly uncertain supra-saturation density equation of state allows for the support of  $2.5 - 2.6 M_{\odot}$  neutron stars without strongly modifying the properties (radius, tidal deformability, and moment of inertia) of  $\sim 1.4 M_{\odot}$  neutron stars. In our analysis, only the softest equations of state are eliminated under this scenario. However, the properties of neutron stars with masses  $\sim 2.0 M_{\odot}$  are significantly different under the two competing assumptions that the GW190814 secondary was a black hole or a neutron star.

PACS numbers: 21.30.-x, 21.65.Ef,

*Introduction*— Recently, the LIGO/Virgo Collaboration (LVC) has reported measurements [1] of gravitational waves resulting from a  $2.50 - 2.67 M_{\odot}$  “mass-gap” object [2] in binary coalescence with a heavy ( $22.2 - 24.3 M_{\odot}$ ) companion black hole. Not only are the mass ratio of  $q = 0.112_{-0.009}^{+0.008}$  and inferred merger rate of  $1 - 23 \text{ Gpc}^{-3} \text{ yr}^{-1}$  challenging to describe [1, 3, 4] with traditional binary evolutionary models, but taken at face value, the mass-gap secondary component in the observation represents the discovery of either the heaviest known neutron star (NS) or the lightest known black hole (BH), though see Ref. [5] for an alternative scenario in which the source of GW190814 is conjectured to be a normal NSBH merger amplified via gravitational lensing. Neither the absence of a measurable tidal deformation signature in the gravitational waveform nor the absence of an electromagnetic counterpart would be unexpected [6] for a NSBH merger at the extreme mass ratio reported in GW190814. However, equation of state inferences [7] based on GW170817 and properties of its electromagnetic counterpart [8–12] suggest that such heavy neutron stars would be challenging to describe with traditional neutron star equations of state founded in nuclear physics models well constrained up to one or two times normal nuclear densities.

Given the highly uncertain nature of matter at densities exceeding two to three times normal nuclear matter

density ( $n_0 = 0.16 \text{ fm}^{-3} = 2.4 \times 10^{14} \text{ g/cm}^3$ ), where there exists no theoretical description of the strong interaction with controlled uncertainties, in this work we explore the extreme scenario in which the high-density equation of state is maximally stiff and therefore can support the heaviest neutron stars. Our low-density equation of state is constrained by nuclear theory and experiment as well as recent radius and tidal deformability measurements of  $\sim 1.4 M_{\odot}$  neutron stars, while the transition region to the maximally stiff equation of state is varied between  $2-4n_0$ . We explore the minimum transition density required to support  $2.5 - 2.6 M_{\odot}$  neutron stars and find that it lies in the region  $n \sim 2.5n_0$ , which is below the central density of neutron stars with masses  $M \sim 1.4 M_{\odot}$ . Nevertheless, we find that the existence of massive  $2.5 - 2.6 M_{\odot}$  neutron stars does not strongly constrain the bulk properties of typical lighter neutron stars, and only the softest equations of state with small radii and tidal deformabilities are excluded. In contrast, the radii and tidal deformabilities of heavy neutron stars with  $M \sim 2.0 M_{\odot}$  differ more significantly under the two competing scenarios that the secondary component of GW190814 is a black hole or a neutron star.

*Bayesian modeling of the neutron star equation of state*— Experimentally measured nuclear binding energies and bulk oscillation modes constrain [13, 14] the nuclear equation of state around normal nuclear density  $n_0$  for matter consisting of nearly equal numbers of neutrons and protons. Neutron-rich matter, on the other hand, is challenging to produce and study in the laboratory, and therefore the principal nuclear physics constraints on the neutron star equation of state rely in one way or another on nuclear theory models, which nowa-

\* ylim@mpi-hd.mpg.de

† anirbanb@stat.tamu.edu

‡ holt@physics.tamu.edu

§ debdeep@stat.tamu.edu

days have a firm foundation in chiral effective field theory [15–17], the low-energy realization of quantum chromodynamics. Previously, we have constructed [18, 19] Bayesian posterior probability distributions for the neutron star equation of state that incorporate constraints from chiral effective field theory [20, 21] and experiment [22, 23]. When these models were extrapolated to high densities, the maximum neutron star mass was found to be  $M \simeq 2.3 M_\odot$ . Numerous other works have employed chiral effective field theory to study the neutron matter equation of state [24–32], neutron star radii [33–35], tidal deformabilities [36–38], and moments of inertia [39, 40]. In describing the properties of the heaviest neutron stars, whose central densities can reach up to  $n = 5\text{--}10n_0$ , all of these models perform extrapolations into regions where the composition and dynamics are poorly understood.

We take as a model for the low-density equation of state a Taylor series expansion in the Fermi momentum  $k_F \sim n^{1/3}$ . This is justified since the bulk nuclear matter equation of state is parametrized by baryon number densities with polytropic index [41, 42] even in the presence of quark matter or phase transitions. The energy density functional for neutron star matter is built from both the pure neutron matter and isospin-symmetric nuclear matter equations of state, interpolated to beta equilibrium conditions ( $\mu_n = \mu_p + \mu_e$ ) enforcing a well-justified [43] quadratic dependence on the proton-neutron asymmetry parameter  $\delta = (n_n - n_p)/(n_n + n_p)$ :

$$\mathcal{E}(n, \delta) = \frac{1}{2m} \tau_n + \frac{1}{2m} \tau_p + [1 - \delta^2] f_s(n) + \delta^2 f_n(n), \quad (1)$$

where  $\tau_n$  ( $\tau_p$ ) is the neutron (proton) kinetic energy densities and  $f_s$  ( $f_n$ ) refers to the isospin-symmetric nuclear matter (pure neutron matter) potential energy density expanded as follows:

$$f_s(n) = \sum_{i=0}^3 a_i n^{(2+i/3)}, \quad f_n(n) = \sum_{i=0}^3 b_i n^{(2+i/3)}. \quad (2)$$

In Eq. (2) the isospin-symmetric nuclear matter coefficients  $\vec{a} = \{a_0, a_1, a_2, a_3\}$  are obtained by fitting to 10 equation of state calculations in chiral effective field theory [20] up to the density  $2n_0$ . We have shown in previous works [18] that lowering the maximum fitting density to  $1.5n_0$  does not qualitatively modify our prior distributions. We then implemented experimental likelihood functions involving the  $\{a_0, a_1, a_2, a_3\}$  parameters from empirical nuclear matter properties, such as the saturation energy, saturation density, incompressibility, and skewness averaged over 205 realistic mean field models fitted to the binding energies and bulk properties of finite nuclei [13]. For the parameters  $\vec{b} = \{b_0, b_1, b_2, b_3\}$  entering in the pure neutron matter energy density functional  $f_n(n)$ , we first fit to a set of 10 chiral effective field theory neutron matter calculations [20] up to the density  $2n_0$ . The resulting multivariate distribution is then refined by imposing nuclear experimental constraints on the isospin-asymmetry energy at saturation density and

its higher-order derivatives in the density [21, 44]. In all of our neutron star structure models, we construct a realistic outer and inner crust using the same parameters ( $\vec{a}, \vec{b}$ ) in a unified way implementing the liquid drop model as explained in more detail in Ref. [45].

To explore the widest range of maximum neutron star masses, we extend this previous model for the equation of state probability distribution to include a transition to the maximally-stiff equation of state consistent with relativity, defined when the speed of sound is equal to the speed of light. The transition density  $n_t$  is taken to have a uniform prior in the range  $2n_0 < n_t < 4n_0$ . A critical density beyond  $4n_0$  is of course possible, but we find that it gives no significant modification to the equation of state prior. Formally, we employ a second-order phase transition where the phase transition starts at  $\mathcal{E} = \mathcal{E}_1$  and ends at  $\mathcal{E} = \mathcal{E}_2$ . Beyond  $\mathcal{E}_2$ , the speed of sound is assumed to be equal to the speed of light, and thus the pressure and energy density have a linear relation. Between  $\mathcal{E}_1$  and  $\mathcal{E}_2$ , the speed of sound is assumed to increase linearly as a function of energy density:

$$c_s^2(\mathcal{E}) = c_1^2 + (1 - c_1^2) \frac{\mathcal{E} - \mathcal{E}_1}{\Delta\mathcal{E}}, \quad \Delta\mathcal{E} = \mathcal{E}_2 - \mathcal{E}_1. \quad (3)$$

The pressure between the phase transition density is then obtained from the integration of the speed of sound:

$$P = P_1 + c_1^2(\mathcal{E} - \mathcal{E}_1) + \frac{(1 - c_1^2)}{2\Delta\mathcal{E}}(\mathcal{E} - \mathcal{E}_1)^2, \quad (4)$$

where  $\Delta\mathcal{E} = \frac{\mathcal{E}_1}{10}$ .

The approach described above defines the prior distribution  $\pi(\cdot)$  associated with the neutron star equation of state parameters  $\theta = (\vec{a}; \vec{b})^T$ . We construct Bayesian posterior probability distributions as follows. Having observed neutron star tidal deformabilities associated with GW170817 [7, 46–48] and simultaneous mass-radius measurements [49, 50] of PSR J0030+045 from the NICER mission, the posterior distribution of  $\theta$  is proportional to  $\mathcal{L}(\theta) \pi(\theta)$ , where

$$\mathcal{L}(\theta) = \left\{ \prod_{i=1}^2 \mathcal{L}_i^{MR}(\theta) \right\} \left\{ \prod_{i=1}^2 \mathcal{L}_i^{M\Lambda}(\theta) \right\}, \quad (5)$$

is the likelihood function of  $\theta$ . In Eq. (5),  $\mathcal{L}_i^{MR}(\theta)$  for  $i = 1, 2$  denotes the likelihood contribution from the two NICER mass-radius measurements, and  $\mathcal{L}_i^{M\Lambda}(\theta)$  for  $i = 1, 2$  denotes the same from the two LIGO mass-tidal deformability measurements. Since these are four independent measurements, the likelihood assumes a product form.

We now detail the construction of the  $\mathcal{L}^{MR}$  likelihood (the  $\mathcal{L}^{M\Lambda}$  terms are similarly derived and we omit the details here). We first introduce some notation to connect the parameter  $\theta$  to the NICER mass-radius measurements. Let  $R_\theta(M)$  denote the (unique) radius-versus-mass curve corresponding to the set of parameters in  $\theta$ . Each  $R_\theta(\cdot)$  curve has its own maximum mass  $M_\theta^{\max}$  above

which the neutron star would collapse to a black hole, and hence the domain of  $R_\theta(\cdot)$  is  $(M_\theta^{\min}, M_\theta^{\max})$ , where in all cases we take  $M_\theta^{\min} = 1.0 M_\odot$ . The exact choice of  $M_\theta^{\min}$  is not particularly crucial, since neither NICER nor LIGO measurements have significant statistical weight around  $1 M_\odot$ . The main purpose of this additional notation is to provide a prescription to randomly generate a  $(M, R)$  pair *a priori*, which proceeds by (i) sampling  $\theta \sim \pi$ , (ii) given  $\theta$ , sampling  $M$  uniformly between  $(M_\theta^{\min}, M_\theta^{\max})$ , and (iii) setting  $R = R_\theta(M)$ . The uniform generation of  $M$  is justified since the equation of state is agnostic about the location on an  $R(M)$  curve.

Although the correlated uncertainty corresponding to either NICER measurement resembles a tilted ellipse, a closer inspection of the contour plots reveal departures from normality. As a result, we refrain from using a parametric Gaussian likelihood function, and instead build a non-parametric likelihood using a kernel density estimator (kde). Specifically, we separately fit kernel density estimators  $\hat{f}_1$  and  $\hat{f}_2$  to the  $(M, R)$  posterior samples corresponding to Fig. 7b of Ref. [49] and Fig. 19 (“ST+PST”) of Ref. [50]. We used the R package `ks` to fit the kde, employing a Gaussian kernel and the bivariate smoothed cross-validation estimator for the bandwidth matrix. Then, we consider an “average” of these fitted densities over an  $R(M)$  curve as the corresponding likelihood, i.e., for  $i = 1, 2$ ,

$$\mathcal{L}_i^{MR}(\theta) = \int_{M_\theta^{\min}}^{M_\theta^{\max}} \hat{f}_i(M, R_\theta(M)) \frac{dM}{M_\theta^{\max} - M_\theta^{\min}}. \quad (6)$$

Next, we describe how we incorporate the secondary “mass-gap” object into our likelihood function. That its distribution is constrained in the interval  $2.50 - 2.67 M_\odot$  makes it a candidate for either the lightest BH or the heaviest NS ever observed. From Fig. 4 of [7], the distribution of the secondary mass  $M_s$  resembles a Gaussian distribution  $N(\mu_s, \sigma_s^2)$  with mean and 90% intervals given by  $2.59_{-0.08}^{+0.08}$ . This leads to  $\mu_s = 2.59$  and  $\sigma_s = 0.048636$ . Hence, for a given value of  $\theta$  from the equation of state, the secondary object is realizable as a neutron star with probability given by

$$\mathbb{P}(M_s \leq M_\theta^{\max}) = \Phi\left(\frac{M_\theta^{\max} - \mu_s}{\sigma_s}\right), \quad (7)$$

where  $\Phi(\cdot)$  denotes the standard Gaussian cumulative distribution function,  $\Phi(x) = \int_{-\infty}^x (2\pi)^{-1/2} e^{-x^2/2} dx$ . Eq. (7) then defines the likelihood of the object assuming it to be a neutron star, denoted  $\mathcal{L}_s^{\text{NS}}(\theta)$ , which when multiplied with  $\mathcal{L}(\theta)$  defined in Eq. (5) gives the overall likelihood for  $\theta$ . Similarly, if we assume the object is a black hole, then the likelihood involves the probability given by  $\mathcal{L}_s^{\text{BH}}(\theta) := 1 - \Phi\{(M_\theta^{\max} - \mu_s)/\sigma_s\}$ .

*Results*— In Fig. 1 we show the mass and radius probability distributions based on the Bayesian analysis described above. In all subpanels of Fig. 1 the green and blue contours represent the 68% (solid lines) and 95% (dashed lines) credibility bands obtained from our kernel

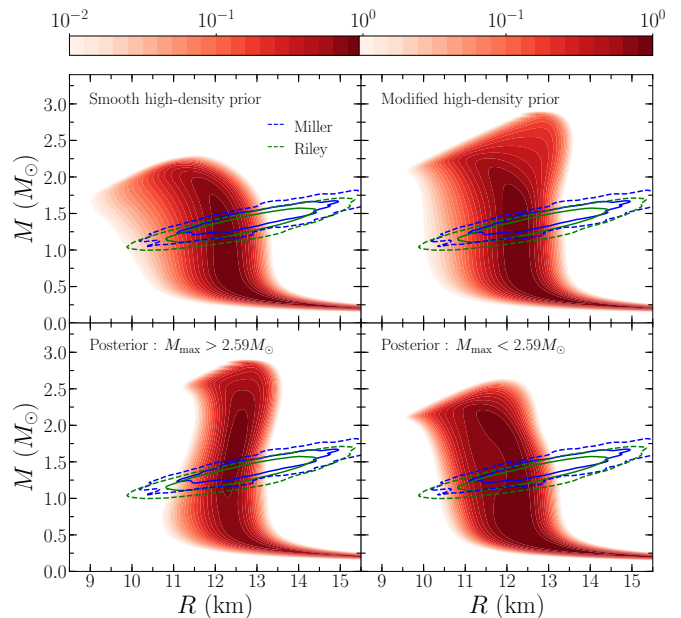


FIG. 1. (Color online) Mass and radius probability distributions for the (top-left) prior without high-density extrapolation, (top-right) prior with high-density extrapolation, (bottom-left) posterior supporting  $\sim 2.6 M_\odot$  neutron stars, and (bottom-right) posterior not supporting  $\sim 2.6 M_\odot$  neutron stars. The green [50] and blue [49] contours represent the NICER 68% (solid) and 95% (dashed) credibility bands.

density estimators associated with the Riley *et al.* [50] and Miller *et al.* [49] analyses of NICER x-ray waveform data from PSR J0030+045. The top-left figure is our previous prior [18] without a high-density extrapolation, the top-right panel is our new prior with uniformly varying transition density  $2n_0 < n_t < 4n_0$ . In order to support  $\sim 2.6 M_\odot$  neutron stars, we find that the transition density must satisfy  $n_t < 2.6n_0$ , indicating that the relatively soft neutron star equations of state predicted by chiral effective field theory must become fairly stiff soon after their natural breakdown scale in the range  $1 - 2n_0$ . We see that the inclusion of the maximally stiff equation of state at high densities naturally leads to much larger maximum neutron star masses, up to  $M_{\max} = 2.9 M_\odot$  for the lowest value of the transition density considered  $n_t = 2n_0$ . We note that this new maximum neutron star mass of  $M_{\max} = 2.9 M_\odot$  is almost certainly unphysical since it lies above the total mass  $M_{\text{tot}} \simeq 2.7 M_\odot$  of the GW170817 remnant, which is expected [51] to have collapsed to a black hole after being supported initially through differential rotation. The bottom-left and bottom-right panels of Fig. 1 represent the posterior mass-radius probability distributions under the assumption that the secondary in GW190814 was a neutron star or a black hole, respectively. Interestingly, we see that for typical neutron stars with masses  $M \sim 1.4 M_\odot$ , the distribution of radii is not strongly different under the two interpretations of the GW190814

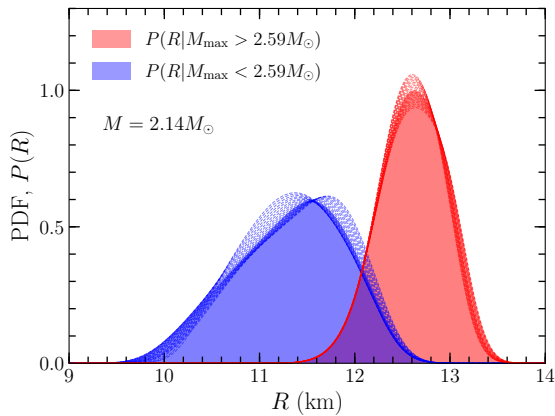


FIG. 2. (Color online) Radius distribution for a heavy neutron star with mass  $2.14 M_{\odot}$  (shaded) under the two assumptions that the GW190814 secondary was a black hole (blue) or a neutron star (red). The dashed lines correspond to varying neutron star masses in the range  $2.04 - 2.24 M_{\odot}$  with spacing  $\Delta M = 0.01 M_{\odot}$ .

secondary. This is due to the fact that the bulk properties of the average neutron star are strongly correlated [18, 52, 53] with the pressure of beta-equilibrium matter at the density  $n = 2n_0$ , which is close to the regime where nuclear physics places strong constraints on the equation of state. However, we do observe that the existence of massive ( $2.5 - 2.6 M_{\odot}$ ) neutron stars would rule out the softest equations of state.

Our previous finding [18] for the radius of a  $1.4 M_{\odot}$  neutron star at the 95% credibility level was  $10.3 \leq R_{1.4} \leq 12.9$  km with the most probable radius as 12.2 km. Including the new kde constraints from the two NICER and GW170817 analyses now give at the 95% credibility level  $10.7 \leq R_{1.4} \leq 12.8$  km under the assumption  $\mathcal{L}_s^{\text{BH}}(\theta)$  and  $11.6 \leq R_{1.4} \leq 12.9$  km under the assumption  $\mathcal{L}_s^{\text{NS}}(\theta)$ . Our finding is consistent with the determination of mass and radius from the cooling tail method [54], where the source for the analysis is different. We see from Fig. 1 that heavy neutron stars, such as PSR J0740+6620 with mass  $2.14^{+0.10}_{-0.09} M_{\odot}$  [55], have significantly different radius probability distributions under our two assumptions for the GW190814 likelihood,  $\mathcal{L}_s^{\text{BH}}(\theta)$  and  $\mathcal{L}_s^{\text{NS}}(\theta)$ . In Fig. 2 we show in the shaded regions the posterior probability distributions for the radius of a  $2.14 M_{\odot}$  neutron star under the two assumptions that the GW190814 secondary was a black hole (blue) or a neutron star (red). The notation  $P(R|M_{\text{max}} > 2.59 M_{\odot})$  corresponds to the likelihood assumption  $\mathcal{L}_s^{\text{NS}}(\theta)$  and likewise  $P(R|M_{\text{max}} < 2.59 M_{\odot})$  corresponds to  $\mathcal{L}_s^{\text{BH}}(\theta)$ . The stiff equations of state needed to support the heaviest neutron stars produce a narrow and large neutron star radius at this mass, while softer equations of state lead to statistically significant smaller radii. In Fig. 2 the dashed lines correspond to different heavy neutron star masses ranging from  $2.04 - 2.24 M_{\odot}$  at spacing  $\Delta M = 0.01 M_{\odot}$ . The radius distributions for the lightest neutron stars ex-

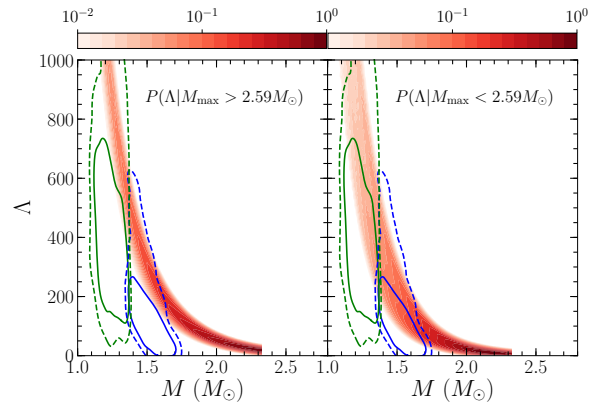


FIG. 3. (Color online) Probability distributions for the tidal deformability versus mass under the two assumptions  $\mathcal{L}_s^{\text{NS}}(\theta)$  (left) and  $\mathcal{L}_s^{\text{BH}}(\theta)$  (right). The blue and green contours show the 68% (solid) and 95% (dashed) credibility bands associated with the primary and secondary in GW170817, respectively.

tend to the smallest radii for both posteriors. We find at the 95% credibility level that the radius of a  $2.14 M_{\odot}$  neutron star is  $10.1 < R_{2.14} < 12.3$  km under the assumption  $\mathcal{L}_s^{\text{BH}}(\theta)$  and  $11.9 < R_{2.14} < 13.2$  km under the assumption  $\mathcal{L}_s^{\text{NS}}(\theta)$ .

In Fig. 3 we show the two posterior probability distributions for the tidal deformability as a function of mass under the two assumption for the likelihood  $\mathcal{L}_s^{\text{BH}}(\theta)$  and  $\mathcal{L}_s^{\text{NS}}(\theta)$ . In both subpanels the blue and green contours denote the 68% (solid lines) and 95% (dashed lines) credibility bands from our kde associated with the primary and secondary components, respectively, of GW170817. In Fig. 4 we show the tidal deformability of a typical  $1.4 M_{\odot}$  neutron star under the assumptions that the GW190814 secondary was a neutron star (red) or black hole (blue). Our previous 95% credibility interval in Ref. [18] was found to be  $136 < \Lambda_{1.4} < 519$ . From the new posterior distribution including NICER and GW170817 measurements as well as the assumption  $\mathcal{L}_s^{\text{BH}}(\theta)$ , we find  $170 < \Lambda_{1.4} < 530$ . Under the opposite scenario,  $\mathcal{L}_s^{\text{NS}}(\theta)$ , we likewise find  $313 < \Lambda_{1.4} < 575$  at the 95% credibility level. There remains a significant overlap between the two distributions, but we observe a broad low tidal deformability region possible only in the absence of heavy neutron stars with masses  $2.5 - 2.6 M_{\odot}$ .

Following the discovery of the double pulsar system J0737-3039, it was suggested [56, 57] that precise radio timing measurements could enable the extraction of spin-orbit coupling effects on the system's periastron advance and hence the moment of inertia of PSR J0737-3039A. The mass of PSR J0737-3039A is precisely known to be  $1.338 M_{\odot}$ , and in Fig. 5 we plot the associated predictions for its moment of inertia assuming that the equation of state can support  $2.5 - 2.6 M_{\odot}$  neutron stars (red) or not (blue). For such a relatively light neutron star, there is an even smaller difference between the moment of inertia probability distributions under the two assumptions

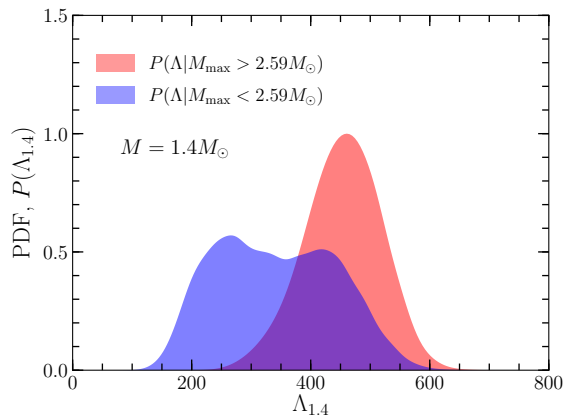


FIG. 4. (Color online) Probability distributions for the tidal deformability of a  $1.4 M_{\odot}$  neutron star under the assumption that the GW190814 secondary was a black hole (blue) or a neutron star (red).

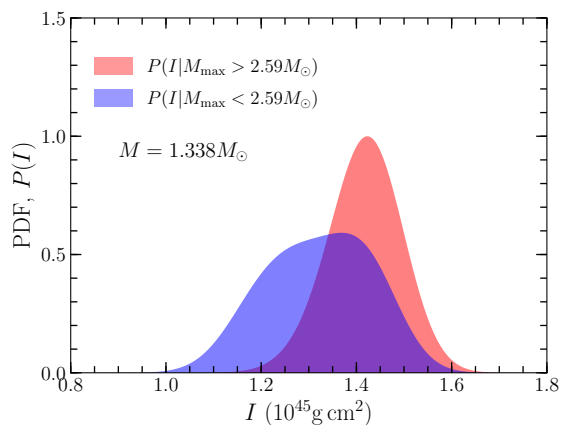


FIG. 5. (Color online) Probability distributions for the moment of inertia of PSR J0737-3039A with mass  $1.338 M_{\odot}$  under the two assumptions that the GW190814 secondary was a black hole (blue) or a neutron star (red).

$\mathcal{L}_s^{\text{BH}}(\theta)$  and  $\mathcal{L}_s^{\text{NS}}(\theta)$ . Previously, we found [39] that at the 95% credibility level the moment of inertia of J0737-3039A should lie in the range  $1.04 \times 10^{45} < I_{1.338} < 1.51 \times 10^{45} \text{ g cm}^2$ . In our revised modeling, including NICER and GW170817 data, we now find a new statistical range  $1.09 \times 10^{45} < I_{1.338} < 1.53 \times 10^{45} \text{ g cm}^2$

under the assumption  $\mathcal{L}_s^{\text{BH}}(\theta)$  and  $1.25 \times 10^{45} < I_{1.338} < 1.56 \times 10^{45} \text{ g cm}^2$  under the assumption  $\mathcal{L}_s^{\text{NS}}(\theta)$ . After accounting for the NICER likelihood functions, we predict a somewhat larger moment of inertia for  $1.338 M_{\odot}$  as well as a reduced statistical uncertainty.

*Summary*— The existence of heavy neutron stars with masses  $2.5 - 2.6 M_{\odot}$  are a challenge to explain with equations of state smoothly extrapolated from the low-density regime ( $1 - 2n_0$ ) constrained by nuclear physics to the highest density regime ( $5 - 10n_0$ ) encountered in neutron star cores. We have demonstrated that a modification of the highly uncertain supra-saturation density equation of state allows for the support of  $2.5 - 2.6 M_{\odot}$  neutron stars consistent with state-of-the-art nuclear theory modeling within the framework of chiral effective field theory, nuclear experiments involving medium-mass and heavy isotopes, as well as current observations of neutron star radii and tidal deformabilities, all integrated within a consistent Bayesian statistical framework. While the nature of the secondary in GW190814 cannot be determined within our present modeling (see also Refs. [58–61]), we note that we have observed strong correlations between the maximum neutron star mass and the radii of heavy neutron stars. We suggest that measurements of very massive ( $\sim 2.0 M_{\odot}$ ) neutron star radii (or tidal deformabilities), such as a NICER measurement of the PSR J0740+6620 radius, may provide a useful and strong constraint on the nuclear equation of state at supra-saturation density.

## ACKNOWLEDGMENTS

Y. Lim was supported by the Max Planck Society and the Deutsche Forschungsgemeinschaft (DFG, German Research Foundation) – Project ID 279384907 – SFB 1245. Dr. Pati and Dr. Bhattacharya acknowledge support from NSF DMS (1854731, 1916371) and NSF CCF 1934904 (HDR-TRIPODS). In addition, Dr. Bhattacharya acknowledges NSF CAREER 1653404 for supporting this project. The work of J. W. Holt is supported by the National Science Foundation under Grant No. PHY1652199 and by the U. S. Department of Energy National Nuclear Security Administration under Grant No. de-na0003841. Portions of this research were conducted with the advanced computing resources provided by Texas A&M High Performance Research Computing.

[1] B. P. Abbott *et al.* (LIGO Scientific Collaboration and Virgo Collaboration), *Astrophys. J. Lett.* **896**, L44 (2020).  
 [2] F. Ozel, D. Psaltis, R. Narayan, and J. E. McClintock, *Astrophys. J.* **725**, 1918 (2010).  
 [3] M. Zevin, M. Spera, C. P. Berry, and V. Kalogera, arXiv:2006.14573 (2020).

[4] K. Vattis, I. S. Goldstein, and S. M. Koushiappas, arXiv:2006.15675 (2020).  
 [5] T. Broadhurst, J. M. Diego, and G. F. Smoot, arXiv:2006.13219 (2020).  
 [6] F. Foucart, L. Buchman, M. D. Duez, M. Grudich, L. E. Kidder, I. MacDonald, A. Mroue, H. P. Pfeiffer, M. A. Scheel, and B. Szilagyi, *Phys. Rev. D* **88**, 064017 (2013).

- [7] B. P. Abbott *et al.* (The LIGO Scientific Collaboration and the Virgo Collaboration), *Phys. Rev. Lett.* **121**, 161101 (2018).
- [8] A. Bauswein, O. Just, H.-T. Janka, and N. Stergioulas, *Astrophys. J. Lett.* **850**, L34 (2017).
- [9] B. Margalit and B. D. Metzger, *Astrophys. J. Lett.* **850**, L19 (2017).
- [10] M. Ruiz, S. L. Shapiro, and A. Tsokaros, *Phys. Rev. D* **97**, 021501 (2018).
- [11] L. Rezzolla, E. R. Most, and L. R. Weih, *Astrophys. J. Lett.* **852**, L25 (2018).
- [12] D. Radice, A. Perego, F. Zappa, and S. Bernuzzi, *Astrophys. J. Lett.* **852**, L29 (2018).
- [13] M. Dutra, O. Lourenço, J. S. Sá Martins, A. Delfino, J. R. Stone, and P. D. Stevenson, *Phys. Rev. C* **85**, 035201 (2012).
- [14] M. Dutra, O. Lourenço, S. S. Avancini, B. V. Carlson, A. Delfino, D. P. Menezes, C. Providência, S. Typel, and J. R. Stone, *Phys. Rev. C* **90**, 055203 (2014).
- [15] S. Weinberg, *Physica A* **96**, 327 (1979).
- [16] E. Epelbaum, H.-W. Hammer, and U.-G. Meißner, *Rev. Mod. Phys.* **81**, 1773 (2009).
- [17] R. Machleidt and D. R. Entem, *Phys. Rept.* **503**, 1 (2011).
- [18] Y. Lim and J. W. Holt, *Phys. Rev. Lett.* **121**, 062701 (2018).
- [19] Y. Lim and J. W. Holt, *Eur. Phys. J. A* **55**, 209 (2019).
- [20] J. W. Holt and N. Kaiser, *Phys. Rev. C* **95**, 034326 (2017).
- [21] J. W. Holt and Y. Lim, *Phys. Lett. B* **784**, 77 (2018).
- [22] M. Dutra, O. Lourenço, J. S. Sá Martins, A. Delfino, J. R. Stone, and P. D. Stevenson, *Phys. Rev. C* **85**, 035201 (2012).
- [23] I. Tews, J. M. Lattimer, A. Ohnishi, and E. E. Kolomeitsev, *Astrophys. J.* **848**, 105 (2017).
- [24] K. Hebeler and A. Schwenk, *Phys. Rev. C* **82**, 014314 (2010).
- [25] L. Coraggio, J. W. Holt, N. Itaco, R. Machleidt, and F. Sammarruca, *Phys. Rev. C* **87**, 014322 (2013).
- [26] A. Gezerlis, I. Tews, E. Epelbaum, S. Gandolfi, K. Hebeler, A. Nogga, and A. Schwenk, *Phys. Rev. Lett.* **111**, 032501 (2013).
- [27] A. Carbone, A. Rios, and A. Polls, *Physical Review C* **90**, 054322 (2014).
- [28] C. Drischler, A. Carbone, K. Hebeler, and A. Schwenk, *Phys. Rev. C* **94**, 054307 (2016).
- [29] I. Tews, S. Gandolfi, A. Gezerlis, and A. Schwenk, *Physical Review C* **93**, 024305 (2016).
- [30] M. Piarulli, I. Bombaci, D. Logoteta, A. Lovato, and R. Wiringa, *Phys. Rev. C* **101**, 045801 (2020), arXiv:1908.04426 [nucl-th].
- [31] C. Drischler, K. Hebeler, and A. Schwenk, *Phys. Rev. Lett.* **122**, 042501 (2019).
- [32] C. Drischler, R. Furnstahl, J. Melendez, and D. Phillips, arXiv:2004.07232 (2020).
- [33] K. Hebeler, J. M. Lattimer, C. J. Pethick, and A. Schwenk, *Phys. Rev. Lett.* **105**, 161102 (2010).
- [34] G. Raaijmakers, S. K. Greif, T. E. Riley, T. Hinderer, K. Hebeler, A. Schwenk, A. L. Watts, S. Nissanke, S. Guillot, J. M. Lattimer, and R. M. Ludlam, *Astrophys. J. Lett.* **893**, L21 (2020).
- [35] C. D. Capano, I. Tews, S. M. Brown, B. Margalit, S. De, S. Kumar, D. A. Brown, B. Krishnan, and S. Reddy, *Nature Astron.* **4**, 625 (2020).
- [36] E. Annala, T. Gorda, A. Kurkela, and A. Vuorinen, *Phys. Rev. Lett.* **120**, 172703 (2018).
- [37] E. R. Most, L. R. Weih, L. Rezzolla, and J. Schaffner-Bielich, arXiv:1803.00549 (2018).
- [38] I. Tews, J. Margueron, and S. Reddy, *Phys. Rev. C* **98**, 045804 (2018).
- [39] Y. Lim, J. W. Holt, and R. J. Stahulak, *Phys. Rev. C* **100**, 035802 (2019).
- [40] S. Greif, K. Hebeler, J. Lattimer, C. Pethick, and A. Schwenk, arXiv:2005.14164 (2020).
- [41] K. Hebeler, J. M. Lattimer, C. J. Pethick, and A. Schwenk, *Astrophys. J.* **773**, 11 (2013).
- [42] S. Greif, G. Raaijmakers, K. Hebeler, A. Schwenk, and A. Watts, *Mon. Not. Roy. Astron. Soc.* **485**, 5363 (2019).
- [43] I. Lagaris and V. Pandharipande, *Nuclear Physics A* **369**, 470 (1981).
- [44] J. Margueron and F. Gulminelli, *Phys. Rev. C* **99**, 025806 (2019).
- [45] Y. Lim and J. W. Holt, *Phys. Rev. C* **95**, 065805 (2017).
- [46] B. P. Abbott *et al.* (LIGO Scientific Collaboration and Virgo Collaboration), *Phys. Rev. Lett.* **119**, 161101 (2017).
- [47] S. De, D. Finstad, J. M. Lattimer, D. A. Brown, E. Berger, and C. M. Biwer, *Phys. Rev. Lett.* **121**, 091102 (2018).
- [48] <https://dcc.ligo.org/LIGO-P1800115/public>.
- [49] M. Miller *et al.*, *Astrophys. J.* **887**, L24 (2019).
- [50] T. E. Riley *et al.*, *Astrophys. J.* **887**, L21 (2019).
- [51] D. Kasen, B. Metzger, J. Barnes, E. Quataert, and E. Ramirez-Ruiz, *Nature (London)* **551**, 80 (2017).
- [52] J. M. Lattimer and M. Prakash, *Astrophys. J.* **550**, 426 (2001).
- [53] M. Tsang, W. Lynch, P. Danielewicz, and C. Tsang, *Phys. Lett. B* **795**, 533 (2019).
- [54] V. F. Suleimanov *et al.*, *Mon. Not. Roy. Astron. Soc.* **466**, 906 (2016).
- [55] H. T. Cromartie *et al.*, *Nature Astronomy* (2019), arXiv:1904.06759.
- [56] A. G. Lyne, M. Burgay, M. Kramer, A. Possenti, R. Manchester, F. Camilo, M. A. McLaughlin, D. R. Lorimer, N. D'Amico, B. C. Joshi, J. Reynolds, and P. C. C. Freire, *Science* **303**, 1153 (2004).
- [57] J. M. Lattimer and B. F. Schutz, *Astrophys. J.* **629**, 979 (2005).
- [58] E. R. Most, L. J. Papenfort, L. R. Weih, and L. Rezzolla, arXiv:2006.14601 (2020).
- [59] H. Tan, J. Noronha-Hostler, and N. Yunes, arXiv:2006.16296 (2020).
- [60] F. Fattoyev, C. Horowitz, J. Piekarewicz, and B. Reed, arXiv:2007.03799 (2020).
- [61] A. Tsokaros, M. Ruiz, and S. L. Shapiro, arXiv:2007.05526 (2020).